Acceleration for Shadow Region Imaging Algorithm with Multiple Scattered Waves for UWB Radars

Ken Akune Shouhei Kidera Tetsuo Kirimoto

Graduate School of Informatics and Engineering, University of Electro-Communications, Tokyo, Japan, akune@secure.ee.uec.ac.jp

Abstract: Ultra-wide band (UWB) pulse radar has high range-resolution, which is applicable to an imaging sensor for household robot or security system. As the past existing works for UWB radar, the SAR (synthetic aperture radar) or RPM (range points migration) method have been already proposed. To enhance the imaging region especially for complex-shaped or multiple objects, the shadow region imaging algorithm based on aperture synthesis for a multiple scattered signal has been proposed. However, this algorithm has a difficulty for real-time processing because it requires large calculation amount due to multiple integration. To resolve this difficulty, this paper proposes high-speed and accurate algorithm for shadow region imaging by combining the former RPM algorithm. The results of the numerical simulation show that the proposed method remarkably decreases the calculation time about 94 times compared to the conventional method, where the accuracy is hold.

Key words: UWB radars, Multiple scattered wave, SAR, Multiple targets, Complex-shaped target, Shadow region.

1 Introduction

Radar imaging systems can observe an object hidden in fog or strong backlight where the optical measurement is hardly applicable. In particular, UWB pulse radar has high range-resolution, and is suitable for the near field imaging sensor such as rescue robots in disaster area, or security system.

Recently, a number of the novel imaging algorithms have been developed aiming at high-speed and high resolution imaging, such as SAR (synthetic aperture radar), SEABED, Envelope, RPM (range points migration) method, and SAR algorithm based on aperture synthesis for a multiple scattered signal are proposed. SAR algorithm is still promising as it creates a stable and accurate image even for targets located in the near field [1]. SEABED achieves direct imaging based on a reversible transform between range points and target boundary [2]. Envelope offers a stable and rapid image without using derivative of the range points [3]. Furthermore, to enhance applicability to various target shapes including complex-shaped and multiple-targets, RPM methods have been proposed [4]. This is based on direct mapping from observed ranges points to target boundary points using accurate DOA estimation. However, these methods suffer from an increased shadow region, because it employs only a single scattered signal for imaging.

Some algorithm based on a multiple scattered solves this problem[5], [6]. Among them, an imaging algorithm based on aperture synthesis for a multiple scattered signal is promising as the method that does not require the priori information of target shapes or surrounding environment.[7]. This method synthesizes the multiple scattered signals along their propagation paths and enhance the imaging range including the area which cannot be seen in the former algorithm. However, this algorithm has a difficulty for real-time processing because it requires large calculation amounts due to the multiple integrals in synthesizing process.

For a substantial solution for such difficulties, this paper proposes high-speed and accurate algorithm for shadow region imaging by combining the former RPM algorithm. As a novelty of this paper, our method dramatically decreases calculation burden by degenerating the triple integral to the single one using the Dirac 's delta function defined by the target points obtained by RPM. In numerical simulations with some examples of complex-shaped or multiple objects, it is shown that the proposed method remarkably reduces the calculation amount without an accuracy distortion.

2 System Model

Fig.1 shows the system model in the 2-dimensional model. It assumes mono-static radar, and an omni-directional antenna that is scanned along the x-axis. It is assumed that the target has an arbitrary shape with a clear boundary, and high conductivity such a metallic objects. The propagation speed of the radio wave c is assumed to be a known constant. A mono-cycle pulse is used as the transmitting signal. The real space in which the target and antenna are located, is expressed by parameters $\boldsymbol{r} = (x, z)$ that

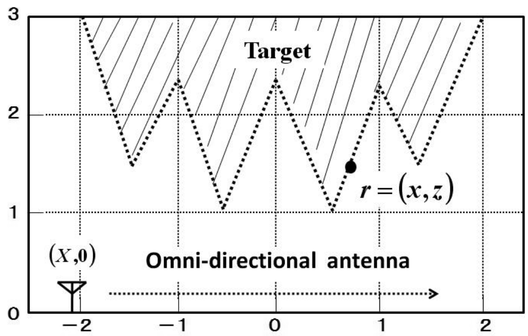

Fig. 1: System model.

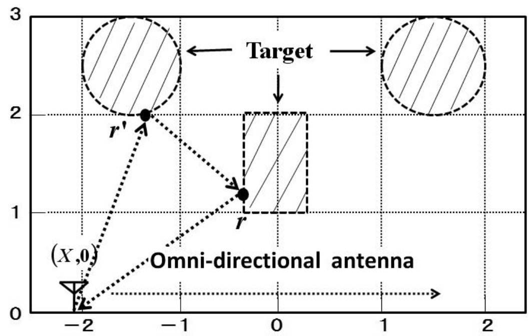

Fig. 3: Target points passed by a double scattered wave.

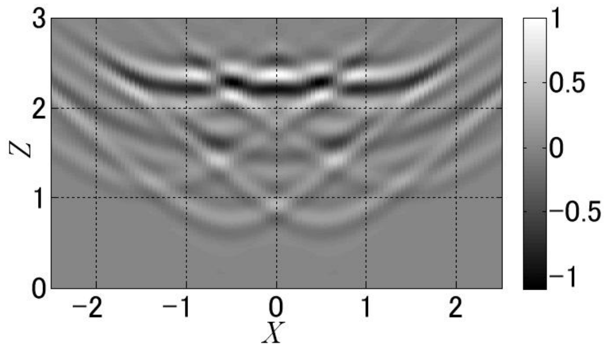

Fig. 2: Output of the Wiener filter $s(X,Z)$ from complex-shaped target as in Fig. 1.

are normalized by the central wavelength of the pulse λ. $z>0$ is assumed for simplicity. $s'(X,Z)$ is defined as the received electric field at the antenna location $(X,0)$, where $Z=\mathrm{c}t/2\lambda$ is expressed by time t. $s(X,Z)$ is defined as the output of Wiener filter with the transmitted waveform[4]. Fig. 2 shows an example of $s(X,Z)$ from complex-shaped target, illustrated as in Fig.2.

3 Conventional Algorithm

The SAR technique is useful as a means of measuring ground level and mineral resource survey. SAR, which is used in the far field, but also holds superior performance in the near field. However, this algorithm suffers from the shadow region especially for a complex-shaped object, and it is inherent problem in the imaging algorithm using only single scattered signals. To resolve this problem, an imaging algorithm based on aperture synthesis for a multiple scattered signal is effective to decrease shadow region. Fig. 3 shows target points passed by a double scattered wave. This algorithm calculates the image $I_2^{\mathrm{S}}(\boldsymbol{r})$ using double scattered waves as,

$$I_2^{\mathrm{S}}(\boldsymbol{r}) = -\int_{\boldsymbol{r'}\in\mathrm{R}}\int_{X\in\Gamma} I_1^{\mathrm{S}}(\boldsymbol{r})\, s\left(X, d_2(X,\boldsymbol{r},\boldsymbol{r'})\right) \mathrm{d}X\mathrm{d}x'\mathrm{d}z', \tag{1}$$

where $\boldsymbol{r'}=(x',z')$, R denotes the region of imaging space, Γ denotes the spatial range of the antenna scanning and $d_2(X,\boldsymbol{r},\boldsymbol{r'}) = \sqrt{(x-X)^2+z^2} + \sqrt{(x'-X)^2+z'^2} + \sqrt{(x-x')^2+(z-z')^2}$. This algorithm uses negative amplitudes of $s(X,Z)$ because the phase of a double scattered wave is the reverse one of a single scattered wave. In this algorithm, $I_1^{\mathrm{S}}(\boldsymbol{r})$ is defined as,

$$I_1^{\mathrm{S}}(\boldsymbol{r}) = \int_{X\in\Gamma} s\left(X, \sqrt{(x-X)^2+z^2}\right)\mathrm{d}X. \tag{2}$$

Eq. (2) shows the image obtained by the conventional SAR processing. Here, we assume that only the positive region of $I_1^{\mathrm{S}}(\boldsymbol{r})$ and $I_2^{\mathrm{S}}(\boldsymbol{r})$ expresses the actual target boundary. Therefore, the final image $I^{\mathrm{S}}(\boldsymbol{r})$ is defined as,

$$I^{\mathrm{S}}(\boldsymbol{r}) = \max\left(\frac{I_1^{\mathrm{S}}(\boldsymbol{r})}{\max\left(I_1^{\mathrm{S}}(\boldsymbol{r})\right)}\ ,\ \frac{I_2^{\mathrm{S}}(\boldsymbol{r})}{\max\left(I_2^{\mathrm{S}}(\boldsymbol{r})\right)}\right). \tag{3}$$

Eq. (3) highlights the image, on which $I_1^{\mathrm{S}}(\boldsymbol{r})$ or $I_2^{\mathrm{S}}(\boldsymbol{r})$ significantly focuses. This method uses only the initial image $I_1^{\mathrm{S}}(\boldsymbol{r})$, and restores target boundary on which double scattered waves pass. That is to say, it is not necessary for imaging to use prior knowledge of the target shape and surrounding environment. Figs. 4 and 5 show the estimated images $I_1^{\mathrm{S}}(\boldsymbol{r})$ as the conventional SAR and $I^{\mathrm{S}}(\boldsymbol{r})$ as the proposed method, respectively. $I^{\mathrm{S}}(\boldsymbol{r})$ increases the reconstructed region compared to the conventional SAR $I_1^{\mathrm{S}}(\boldsymbol{r})$. However, this algorithm has a difficulty for real-time processing because it requires large calculation amounts due to the triple integrals in synthesizing process. The calculation time of this method is 3100 sec with a Xeon 2.40 GHz.

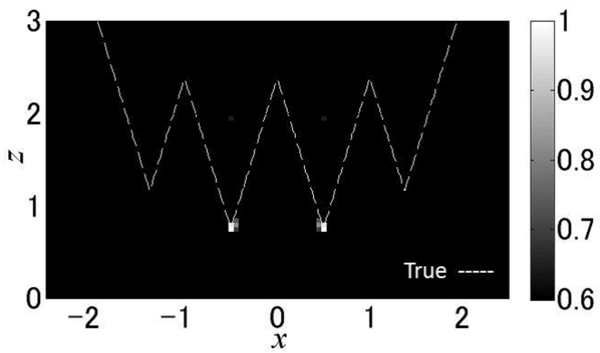

Fig. 4: Estimated image with the conventional SAR method $I_1(\boldsymbol{r})$ for complex-shaped target.

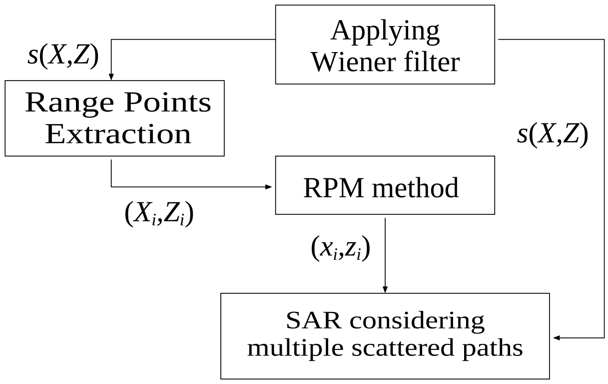

Fig. 6: Flowchart of the propose method.

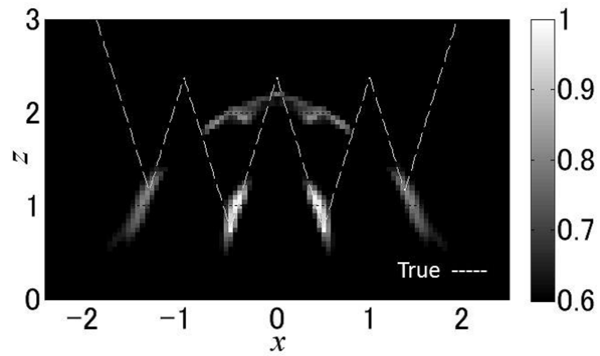

Fig. 5: Estimated image with the conventional $I^{\mathrm{S}}(\boldsymbol{r})$ for the complex-shaped target.

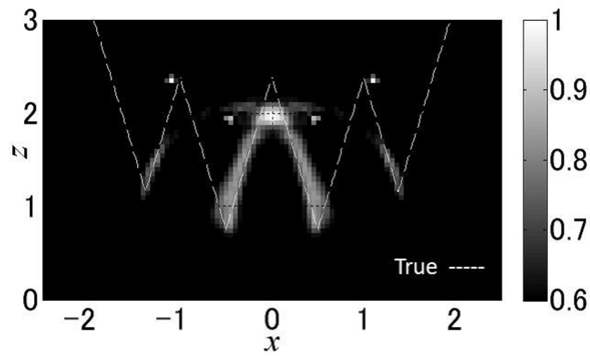

Fig. 7: Estimated image with the proposed method $I^{\mathrm{R}}(\boldsymbol{r})$ for complex-shaped target.

4 Proposed Algorithm

To resolve the previous problem, we propose high-speed algorithm for shadow region imaging by combining the former RPM algorithm. The conventional algorithm uses the SAR image as the initial image, while on the other hand, the proposed algorithm uses the target points obtained by RPM. RPM accomplishes an accurate and high-speed imaging with a single scattered wave, that employs the global characteristic of so-called “ range points ” for accurate DOA estimation in order to apply to the complex or multiple objects [4]. RPM uses the range points (X, Z) which are extracted from local maximum output of Wiener filter.[4]. Also, we calculate the target points (x_i, z_i) corresponding to the range points (X_i, Z_i). By using this algorithm, $I_1^{\mathrm{S}}(\boldsymbol{r})$ in Eq. (1) is redefined as $I_1^{\mathrm{RPM}}(\boldsymbol{r})$,

$$I_1^{\mathrm{RPM}}(\boldsymbol{r}) = \sum_{i=1}^{N} s(X_i, Z_i) \cdot \delta(x - x_i, z - z_i), \quad (4)$$

then, Eq.(1) is reformulated as,

$$I_2^{\mathrm{R}}(\boldsymbol{r}) = -\int_{X \in \Gamma} \sum_{i=1}^{N} s(X_i, Z_i)\, s(X, d_2(X, \boldsymbol{r}, \boldsymbol{r}_i))\, \mathrm{d}X, \quad (5)$$

where N is the number of the range points, $\boldsymbol{r}_i = (x_i, z_i)$ are the target points estimated by RPM. The proposed method can degenerate to the single integral using the Dirac 's delta function calculated by the target points estimated by RPM with a single scattered signal. To synthesize the focused final image as $I^{\mathrm{S}}(\boldsymbol{r})$ with Eq. (3), the initial image obtained by RPM is defined as,

$$I_1^{\mathrm{R}}(\boldsymbol{r}) = \sum_{i=1}^{N} s(X_i, Z_i) \cdot \exp\left(-\frac{(X - x_i)^2 + {z_i}^2}{2\sigma_{\mathrm{s}}^2}\right), \quad (6)$$

where σ_{s} is constant. Also, the final image $I^{\mathrm{R}}(\boldsymbol{r})$ as well as $I^{\mathrm{S}}(\boldsymbol{r})$ is defined as,

$$I^{\mathrm{R}}(\boldsymbol{r}) = \max\left(\frac{I_1^{\mathrm{R}}(\boldsymbol{r})}{\max\left(I_1^{\mathrm{R}}(\boldsymbol{r})\right)}, \frac{I_2^{\mathrm{R}}(\boldsymbol{r})}{\max\left(I_2^{\mathrm{R}}(\boldsymbol{r})\right)}\right). \quad (7)$$

Fig. 6 shows the flowchart of the proposed method. This method also suppresses a false image caused by a unnecessary response due to the range sidelobe of the Wiener filter, because the RPM offers only the accurate target points. Moreover, our method is expected that dramatically decreases calculation amounts because it degenerates the triple integral to the single one.

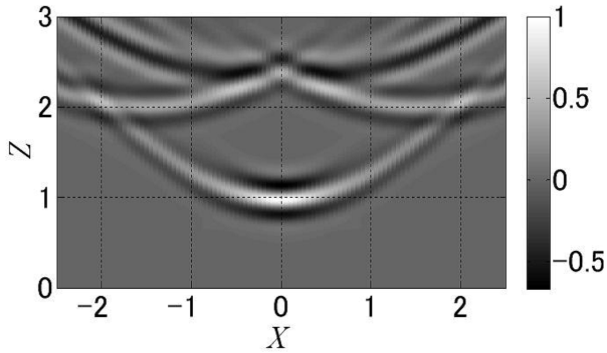

Fig. 8: Output of the Wiener filter $s(X, Z)$ from multiple-targets.

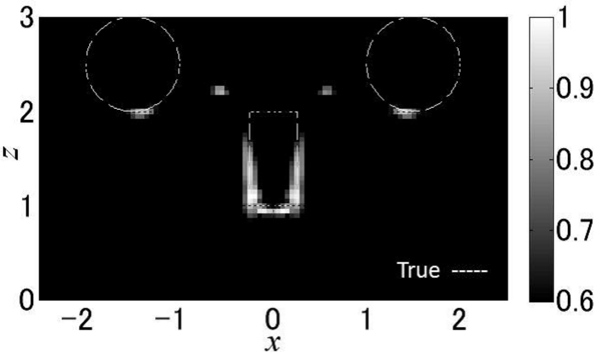

Fig. 9: Estimated image with the conventional method $I^{\mathrm{R}}(\boldsymbol{r})$ for multiple targets.

5 Performance Evaluation in Numerical Simulation

This section presents the performance evaluations of the proposed and conventional methods. Figs. 5 and 7 show the conventional and proposed images $I^{\mathrm{S}}(\boldsymbol{r})$ and $I^{\mathrm{R}}(\boldsymbol{r})$ for complex-shaped target, respectively, when using the same data as in Fig. 2. $\sigma_{\mathrm{s}} = 0.1\lambda$ is set. Both images $I(\boldsymbol{r})$ are normalized by each maximum value. Fig. 7 shows that the proposed method increases the reconstructed region including in the side of the target because this method suppresses unnecessary image due to the range sidelobe of the Wiener filter, which appear in the image of the conventional method.
For a quantitative analysis, the evaluated value is introduced as,

$$\bar{\epsilon} = \frac{\int_{\boldsymbol{r}\in R} \min_{\boldsymbol{p}_{\mathrm{true}}} ||\boldsymbol{r} - \boldsymbol{p}_{\mathrm{true}}||\, |I(\boldsymbol{r})|\, \mathrm{d}\boldsymbol{r}}{\int_{\boldsymbol{r}\in R} |I(\boldsymbol{r})|\, \mathrm{d}\boldsymbol{r}}, \tag{8}$$

where $\boldsymbol{p}_{\mathrm{true}}$ is the true target points. This accuracy is weighted with image intensities. The evaluation value shows $\bar{\epsilon} = 0.027\lambda$ for the conventional method, $\bar{\epsilon} = 0.0092\lambda$ for the proposed method, respectively.. This result quantitatively shows that the proposed method has a significant advantage for the accurate

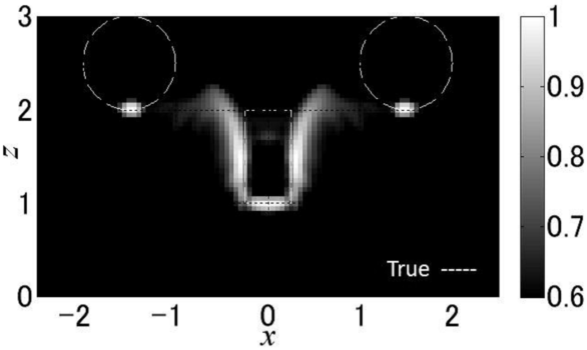

Fig. 10: Estimated image with the proposed method $I^{\mathrm{R}}(\boldsymbol{r})$ for multiple targets.

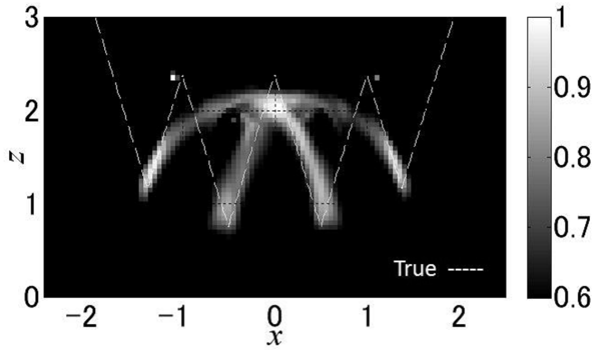

Fig. 11: Estimated image with the proposed method $I^{\mathrm{R}}(\boldsymbol{r})$ for complex-shaped target in noisy case at S/N=30dB.

imaging, and shortens the calculation time about 94 times compared to the conventional method with a Xeon 2.40 GHz. Furthermore, Figs. 9 and 10 show the conventional and proposed images $I^{\mathrm{S}}(\boldsymbol{r})$ and $I^{\mathrm{R}}(\boldsymbol{r})$ for multiple targets, respectively, when using the same data as in Fig. 8. $\sigma_{\mathrm{s}} = 0.1$ is set. The evaluation value shows $\bar{\epsilon} = 0.0712\lambda$ for the conventional method, $\bar{\epsilon} = 0.1157\lambda$ for the proposed method, respectively. This result quantitatively shows that the proposed method holds the accuracy around 0.1λ, which is slightly worsen than that of the conventional method. It should be also noted that this methodshortens the calculation time about 62 times compared to the conventional method with a Xeon 2.40 GHz.

Finally, performance evaluaitons in the noisy case are demonstrated. The Gaussian white noise is added to $s'(X, Z)$. S/N defined as,

$$\mathrm{S/N} = 10\log_{10}\frac{\mathrm{R}_0^2}{\sigma_{\mathrm{noise}}^2}, \tag{9}$$

where $\sigma_{\mathrm{noise}}^2$ is the power density of the noises, and R_0 denotes the maximum power spectrum density of the received signal in the frequency domain. Figs. 11 and 12 show estimated boundaries with the proposed method for complex-shaped and multiple targets, re-

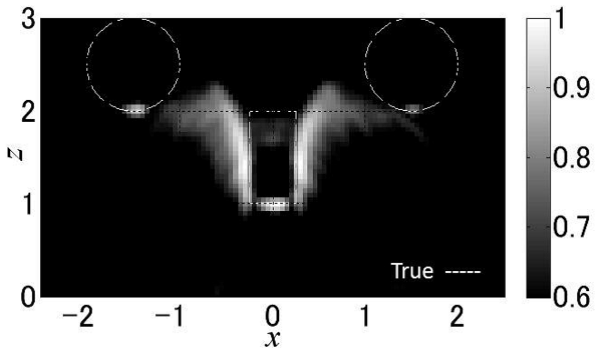

Fig. 12: Estimated image with the proposed method $I^{\mathrm{R}}(\boldsymbol{r})$ for multiple targets in noisy case at S/N=10dB.

spectively. The S/N ratios are 30dB for complex-shaped target and 10dB for multiple targets. Fig. 11 shows that the proposed method also enhances the imaging range while the false images due to random noise components appear above the actual boundary. This is because the random noises are mostly suppressed in the synthesizing processing. Fig. 12 shows that the magnitudes of focused images are relatively weak compared to those in noiseless case. However, the evaluation value shows $\bar{\epsilon} = 0.0121\lambda$ for complex-shaped target, $\bar{\epsilon} = 0.139\lambda$ for multiple targets, respectively. The result shows this proposed method is capable to maintain the performance up to 30dB for complex-shaped target and 10dB for multiple targets.

6 Conclusion

This paper proposed a high-speed imaging algorithm for a multiple scattered signal by using synthesizing process in combination with RPM. The conventional algorithm has the problem that it requires a large computational burden because it employs the triple integrals in synthesizing process. The proposed method efficiently degenerates the multiple integration by using the Dirac 's delta function defined by the target points estimated by the RPM, and dramatically decreased calculation amounts. It was shown that the calculation time for the proposed method was reduced about 94 times compared to the conventional method in complex-shaped target. Also, its image quality was enhanced because this algorithm employs accurate target points obtained by the RPM method.

References

[1] D. L. Mensa, G. Heidbreder and G. Wade, "Aperture Synthesis by Object Rotation in Coherent Imaging," *IEEE Trans. Nuclear Science* vol. 27, No. 2,pp. 989-998, Apr, 1980.

[2] T. Sakamoto, T. Sato, "A Target Shape Estimation Algorithm for Pulse Radar Systems Based on Boundary Scattering Transform," *IEICE Trans.Commun.*, vol.E87-B, no.5, pp. 1357-1365, July, 2004.

[3] S. Kidera, T. Sakamoto, T. Sato, "A Robust and Fast Imaging Algorithm with an Envelope of Circles for UWB Pulse Radars," *IEICE Trans.Commun.*, vol.E90-B, no.7, pp. 1801-1809, July, 2007.

[4] S. Kidera, T. Sakamoto, T. Sato, "Accurate UWB Radar 3-D Imaging Algorithm for Complex Boundary without Wavefront Connections," *IEEE. Trans Geoscience and Remote Sensing*, vol. 48, No. 4,pp. 1993-2004, Apr, 2010.

[5] S. K. Lehmanm and A. J. Devaney, "Transmission mode time-reversal super-resolution imaging," *Acoust. Soc. Am.* 113(5), May, 2003.

[6] J. M. F. Moura, and Y. Jin, "Detection by Time Reversal: Single Antenna," *IEEE Trans. on Signal Process.*, vol. 55,no. 1,pp. 187-201, Jan, 2007

[7] S. Kidera, T. Sakamoto, T. Sato, "Shadow Region Imaging Algorithm Based on Aperture Synthesis with Multiple Scattered Waves for UWB Radars," *Proc. of PIERS 2009* vol. 5, No. 4,pp. 393-396, Aug, 2009.